Biosensors and Bioelectronics ■ (■■■■) ■■■–■■■

Contents lists available at ScienceDirect

Biosensors and Bioelectronics

journal homepage: www.elsevier.com/locate/bios

A fluorescence turn-on biosensor based on graphene quantum dots (GQDs) and molybdenum disulfide (MoS_2) nanosheets for epithelial cell adhesion molecule (EpCAM) detection

Jingyu Shi, Jing Lyu, Feng Tian, Mo Yang *

Interdisciplinary Division of Biomedical Engineering, the Hong Kong Polytechnic University, Hung Hom, Kowloon, Hong Kong, China

ARTICLE INFO

Article history:
Received 17 June 2016
Received in revised form
23 August 2016
Accepted 2 September 2016

Keywords:
Graphene quantum dots (GQDs)
Molybdenum disulfide (MoS_2)
Fluorescence resonance energy transfer (FRET)
Epithelial cell adhesion molecule (EpCAM)

ABSTRACT

This paper presents a "turn-on" fluorescence biosensor based on graphene quantum dots (GQDs) and molybdenum disulfide (MoS_2) nanosheets for rapid and sensitive detection of epithelial cell adhesion molecule (EpCAM). PEGylated GQDs were used as donor molecules, which could not only largely increase emission intensity but also prevent non-specific adsorption of PEGylated GQD on MoS_2 surface. The sensing platform was realized by adsorption of PEGylated GQD labelled EpCAM aptamer onto MoS_2 surface via van der Waals force. The fluorescence signal of GQD was then quenched by MoS_2 nanosheets via fluorescence resonance energy transfer (FRET) mechanism. In the presence of EpCAM protein, the stronger specific affinity interaction between aptamer and EpCAM protein could detach GQD labelled EpCAM aptamer from MoS_2 nanosheets, leading to the restoration of fluorescence intensity. By monitoring the change of fluorescence signal, the target EpCAM protein could be detected sensitively and selectively with a linear detection range from 3 nM to 54 nM and limit of detection (LOD) around 450 pM. In addition, this nanobiosensor has been successfully used for EpCAM-expressed breast cancer MCF-7 cell detection.

1. Introduction

Epithelial cell adhesion molecule (EpCAM) is a glycosylated membrane protein expressed on the surface of circulating tumor cells (CTCs) (Baeuerle and Gires, 2007). EpCAM protein is considered to be the most frequently and intensely studied tumor-associated antigens because of its overexpression in most cancer cells, including colorectal cancer (Dalerba et al., 2007), breast cancer (Gastl et al., 2000), gallbladder cancer (Varga et al., 2004), pancreatic cancer (Fong et al., 2008) and liver cancer (Yamashita et al., 2010). In a perspective view, EpCAM has been regarded as a prognostic tumor biomarker for cancer diagnosis, prognosis and therapy (Baeuerle and Gires, 2007). Previously, cytometry technique, polymerase chain reaction (PCR), or a combination or both approaches have been widely used for EpCAM based CTCs detection (Ntouroupi et al., 2008; Lambrechts et al., 1999). However, these methods suffer from the disadvantages of long analytical time, labor-intensive operation and expensive instruments, which hamper the application of point of care diagnosis (Ntouroupi et al., 2008; Lambrechts et al., 1999; Gubala et al., 2012). Besides, a majority of EpCAM-based diagnostic and therapeutic approaches are relied on anti-EpCAM antibody, which fails to provide objective clinical response because of the large size and instability in physiological environment (Schwartzberg, 2001; Armstrong and Eck, 2003). Therefore, small sized aptamer with the merits of ease of synthesis, good stability, fast tissue penetration and low toxicity has raised much attention as a perfect alternative of antibody (Tan et al., 2013). The specific affinity interaction between aptamer and different biomolecular targets also stimulates the extensively application of aptasensor (Song et al., 2013).

Fluorescence resonance energy transfer (FRET), relying on the energy transfer between donor and acceptor, is a powerful tool to monitor biomolecular interactions in nano-scale. The FRET based aptasensor is very promising due to its direct response and feasible quantification (Choi et al., 2006; Bagalkot et al., 2007; Shi et al., 2015a; Tsang et al., 2016). Traditional FRET pairs, such as fluorescent dyes and proteins, are mainly limited by poor photobleaching resistance and low chemical stability. Novel fluorescence nanoparticles, such as semiconductor quantum dots (QDs) (Zhang et al., 2005) and upconversion nanoparticles (UCNPs) (Ye et al., 2014), are photo-stable fluorescence probes but hampered by the high toxicity for biological applications. The emergence of graphene quantum dots (GQDs) as fluorescence probes perfectly solves these problems (Sun et al., 2013). GQDs are well-confined

* Corresponding author.
E-mail address: Mo.Yang@polyu.edu.hk (M. Yang).

http://dx.doi.org/10.1016/j.bios.2016.09.012
0956-5663/

0D graphene fragments with high brightness, good photo-stability and excellent biocompatibility, which ensure their application as FRET donors in long-term bio-detection (Zhu et al., 2012; Shi et al., 2015b; Qian et al., 2015; Bhatnagar et al., 2016).

In addition, graphene oxide (GO), the water-soluble graphene derivative equipped with super quenching ability, has been used as efficient fluorescence acceptors in FRET assay (Shi et al., 2015c). Recently, much focus has been paid to other 2D materials such as transition metal dichalcogenides (TMD) due to their graphene-analogous structure (Xu et al., 2013; Yang et al., 2015). Among them, molybdenum disulfide (MoS_2) has attracted tremendous attention due to its easy exploitation, unique electronic and optical properties. Single-layered MoS_2 nanosheet is made up of a hexagonal layer of molybdenum atoms sandwiched between two layers of sulfur atoms (Ataca and Ciraci, 2011). Due to its high quenching capability and good biocompatibility, MoS_2 nanosheets started to be used as quenchers in FRET assays for biosensing applications. Zhu et al. (2013) firstly reported the high fluorescence quenching capability of MoS_2 nanosheet for fluorescent dye labelled ssDNA and demonstrated the different affinity to ssDNA versus dsDNA. After that, MoS_2 nanosheet based FRET platforms have been used for protein detection including DNA methyltransferase (MTase) activity (Deng et al., 2015), human a-thrombin (Ge et al., 2014) and prostate specific antigen (PSA) (Kong et al., 2015). However, the current MoS_2 FRET assays mainly used fluorescent dyes as donor molecules. The FRET assay with GQD as donor and MoS_2 as acceptor for protein detection has not been explored.

Herein, we reported a novel GQD-PEG-aptamer/MoS_2 based FRET assay for EpCAM protein detection with GQD as donor and MoS_2 nanosheet as quencher. The FRET assay was established by attachment of GQD labelled aptamer on MoS_2 nanosheets, triggering FRET phenomena due to close proximity between GQD and MoS_2 nanosheets. The fluorescence signal was maintained at "off" status due to the fluorescence quenching of GQD by MoS_2 nanosheets. In the presence of EpCAM protein, the specific affinity between aptamer and EpCAM protein would detach GQD labelled aptamer from MoS_2 surface, which turned "on" the fluorescence signal. By monitoring the change of fluorescence signal, EpCAM protein could be detected sensitively. The proposed FRET assays displayed a linear range from 3 nM to 54 nM with a limit of detection (LOD) around 450 pM.

2. Materials and methods

2.1. Materials

Carboxylated graphene quantum dot (GQD-COOH) solution was purchased from Nanjing XFNANO Materials Tech Co., Ltd. (Nanjing, Jiangsu, China). Molybdenum disulfide (MoS_2) nanosheets were purchased from Nanjing Mknano Science and Technology Co., Ltd. (Nanjing, Jiangsu, China). Amine-PEG-Amine (MW = 2000) was purchased from Laysan Bio, Inc. (Arab, Al, USA). 1-Ethyl-3-(3-dimethyl-aminopropyl) carbodiimide (EDC) and N-hydroxysulfosuccinimide (Sulfo-NHS) were purchased from Sigma Aldrich (St. Louis, Mo, USA). All of these chemicals were used as received without further purification. Aptamer was synthesized and purified by Integrated DNA Technologies (IDT) Inc. (Coralville, IA, US). A 48-base hairpin-structured aptamer modified with carboxyl group was used as the probe (5′-/5carboxy1/-CAC TAC AGA GGT TGC GTC TGT CCC ACG TTG TCA TGG GGG GTT GGC CTG-3′) (Song et al., 2013). EpCAM recombinant human protein (hIgG1-Fc Ta) purchased from Sino biological Inc. (North Wales, PA, USA) was used as EpCAM-positive protein target. All the aptamer and protein were dissolved in ultrapure water to prepare stock solution.

2.2. Synthesis of PEGylated GQDs

Briefly, 2.4 mg of 1-Ethyl-3-(3-dimethyl-aminopropyl) carbodiimide (EDC) and 3.6 mg of N-hydroxysulfosuccinimide (Sulfo-NHS) were added into 1 mL carboxylated graphene quantum dot (GQD-COOH) solution (1 mg/mL) and the mixture was stirred for 15 min. Then, 10% Amine-PEG-Amine diluted with PBS was added and incubated with activated GQD-COOH overnight at room temperature Finally, the PEGylated GQDs solution was purified and concentrated by ultrafiltration (Amicon Ultra-0.5, 3KD, Millipore). The possible large-sized aggregates could be filtered out by using microporous millipore membrane (0.22 μm) to get small GQD-PEG particles.

2.3. Synthesis of aptamer conjugated PEGylated GQDs

Carboxyl modified aptamer was then covalently conjugated onto the amine functionalized GQDs-PEG through EDC/NHS method. Initially, the carboxyl modified aptamer was pretreated with EDC/NHS for 15 min. After that, the activated aptamer with final concentration of 1.95 μM was added into amine functionalized GQDs-PEG solution. The mixture was then shaken overnight at room temperature. In order to remove excessive EDC, NHS and aptamer, the final product, GQD-PEG-aptamer, was purified and concentrated by ultrafiltration (Amicon Ultra-0.5, 30 KD, Millipore).

2.4. FRET assay establishment and EpCAM protein detection

Fluorescence spectra of FRET quenching efficiency and EpCAM protein detection were recorded by an Edinburgh FLSP920 spectrophotometer equipped with a 450 W steady-state xenon lamp at room temperature. In a typical experiment, the final product of GQD-PEG-aptamer (50 μL) was incubated with MoS_2 nanosheets (50 μL) against a series of final concentrations ranging from 10 μg/mL to 400 μg/mL. After 20 min incubation, the sample was measured with the excitation and emission wavelengths fixed at 360 nm and 466 nm, respectively. For EpCAM protein detection, GQD-PEG-aptamer/MoS_2 nanocomplex was incubated with an increasing concentration of target protein (3 nM, 9 nM, 18 nM, 36 nM, 54 nM). After 2 h incubation at 37 °C in the dark environment, the fluorescence signal was measured, respectively. The control experiments were conducted by measuring the fluorescence signal of sample after addition of the same volume of PBS. All the fluorescence spectra were recorded under the same condition.

2.5. Characterization

The morphology and size of GQDs, GQD-PEG and MoS_2 nanosheets were characterized using a JEOL-2100F transmission electron microscopy (TEM) equipped with an Oxford Instrument EDS system, operating at 200 kV. The absorption spectra of GQDs, GQD-PEG, MoS_2 nanosheets were characterized by a UV–vis spectrophotometer (Ultrospec 2100 pro). The Zeta potential and size distribution of MoS_2 nanosheets were determined at neutral pH environment with a Zetasizer Nano Z system from Malvern Instruments Ltd.

3. Results

3.1. Mechanism of GQD-PEG-aptamer/MoS_2 based FRET biosensor

The sensing mechanism of GQD-PEG-aptamer/MoS_2 based FRET biosensor for EpCAM protein detection is shown in Scheme 1

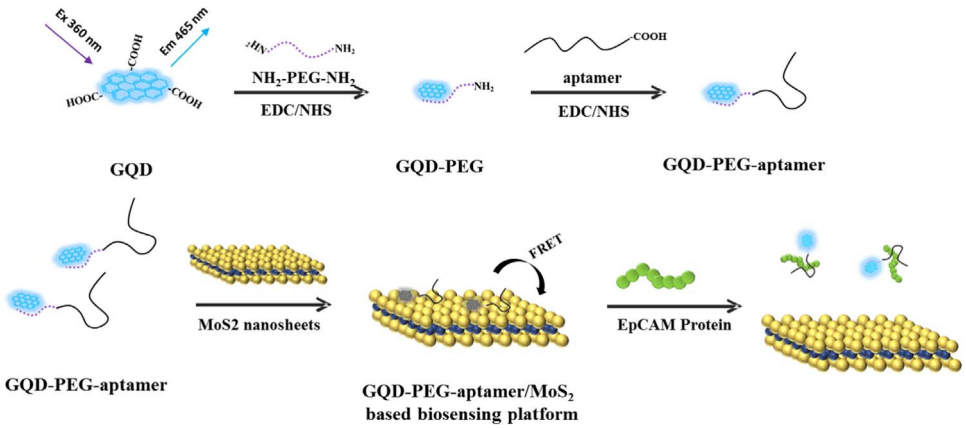

Scheme 1. The sensing mechanism of GQD-PEG-aptamer/MoS_2 based FRET biosensor for EpCAM protein detection.

GQD is utilized as the FRET donor, which can emit intense blue light at 466 nm under UV light excitation of 360 nm. 2D MoS_2 nanosheets with good quenching ability are served as the sensing platform and the FRET acceptor. In order to prevent the non-specific absorption, amine functionalized PEG is firstly conjugated onto GQD through EDC/NHS method. PEGylated GQD can also emit much stronger fluorescence as compared to bare GQD due to the quantum confinement effect. Carboxylated aptamer is then conjugated onto PEGylated GQD by EDC/NHS chemistry. The sensing platform is realized by the adsorption of aptamer on MoS_2 nanosheets via van der walls force, which brings GQD and MoS_2 into close proximity. Under 360 nm excitation, the fluorescence of GQD is highly quenched by MoS_2 due to the ultra-high quenching capability of MoS_2. In the presence of EpCAM protein, the stronger binding affinity between aptamer and EpCAM protein could detach GQD labelled EpCAM aptamer from MoS_2 nanosheets, leading to the restoration of fluorescence signal. By monitoring the change of fluorescence signal, the target EpCAM protein can then be detected.

3.2. Characterization of GQDs and MoS_2 nanosheets

TEM experiments were performed to characterize the morphology and size of PEGylated graphene quantum dots and MoS_2 nanosheets. As shown in Fig. 1a, bare GQDs are homogeneous with diameter of 2.8 ± 0.5 nm (Fig. 1b). After PEGylation of GQDs, the collected GQDs-PEG are monodispersed with an obviously increased size (Fig. 1c). The average size increased to 4.2 ± 0.8 nm (Fig. 1d). To further confirm the conjugation between GQD and PEG, UV–vis absorption spectra were measured before and after PEGylation (Fig. 1e). Before PEGylation, GQD shows an absorption peak at 336 nm, which is assigned to n-π^* transition of C=O. After PEGylation, the adsorption curve of GQD-PEG notably shifted to the left without the peak at 336 nm. This blue shift can be explained by the PEG surface passivation of GQD. FTIR spectra before and after PEGylation were also measured. As shown in Fig. S1, the characteristic bands of GQD at 1630 cm^{-1} (aromatic C=C bond) and PEG at 2916 cm^{-1} (C–H stretch) and 1079 cm^{-1} (C–O–C stretch) appeared simultaneously on GQD-PEG spectrum, which demonstrated the successfully conjugation of PEG on GQD. Fig. 1f shows MoS_2 nanosheets with graphene-like 2D structure, which makes them to be ideal nano-sensing platforms with high biomolecule loading rate. The average size of MoS_2 nanosheets is around 345 nm (Fig. S2). Selective area electron diffraction (SAED) on the MoS_2 nanosheets indicates the MoS_2 nanosheets are polycrystalline with some discrete diffraction spots arranged on the concentric rings (Inlet, Fig. 1f). The Zeta potential of MoS_2 nanosheets is around -38 mV, indicating their negative surface charge (Fig. S3). Fig. 1g shows the obtained graphene-PEG-aptamer-MoS_2 composites in TEM image. The enlarged high resolution TEM (HRTEM) image clearly shows that functionalized GQDs are well adsorbed on the surface of MoS_2 nanosheets. Energy dispersive X-ray (EDX) spectrum confirms the formation of graphene-PEG-aptamer/MoS_2 composites with the presence of elements of Mo, S, C, O and P. Here, element of P is from aptamer on GQD surface (Fig. S4).

3.3. Emission spectra of GQDs-PEG and adsorption spectra of MoS_2 nanosheets

Under 365 nm laser excitation, both GQDs and GQDs-PEG emit blue light with a slight emission peak shift from 468 nm (GQDs) to 478 nm (GQD-PEGs) (Fig. 2a). Both GQDs and GQDs-PEG disperse well in water solution due to the abundant oxygen-containing functional groups or hydrophilic PEG chains on the surface, which is demonstrated by the uniform blue color distribution in GQD solution. The PL intensity of GQDs-PEG is obviously higher than bare GQDs with a brighter blue emission in the photographs (Inlet, Fig. 2a). The enhanced PL intensity is attributed to the surface passivation of GQDs with more quantum confinement of emission energy trapped on GQDs (Shen et al., 2011). The absorption spectrum of MoS_2 nanosheets mostly centers in UV region and extends the adsorption band to the NIR range. The spectra overlapping between emission spectra of GQDs and absorption spectra of MoS2 nanosheets ensured the feasibility of this FRET biosensor (Fig. 2b).

3.4. Construction of GQD-PEG-aptamer/MoS_2 based FRET biosensor

To establish a FRET assay with high quenching efficiency, it is important to optimize the ratio between the donor molecules and the quencher molecules. In order to get the optimal ratio between GQD-PEG-aptamer and MoS_2 nanosheets for maximum quenching efficiency, 50 μL solution of as-prepared GQD-PEG-aptamer with fixed concentration of 1 mg/mL was incubated with 50 μL of a series of concentrations of MoS_2 nanosheets ranging from 10 μg/mL to 400 μg/mL. The fluorescence signals of GQD-PEG-aptamer/MoS_2 nanocomplex were then measured for this series of donor to acceptor ratios from 100 to 2.5. The fluorescence intensity of GQD-PEG-aptamer solution mixed with the same volume of PBS was regarded as control group (F_0). The photoluminescence spectra of GQD-PEG-aptamer/MoS_2 composite at different ratio is shown in Fig. 3a. It was observed that the fluorescence signal of GQD-PEG-aptamer gradually decreased with the increasing concentrations of MoS_2 nanosheets from 10 μg/mL to 400 μg/mL. This fluorescence quenching was induced by the

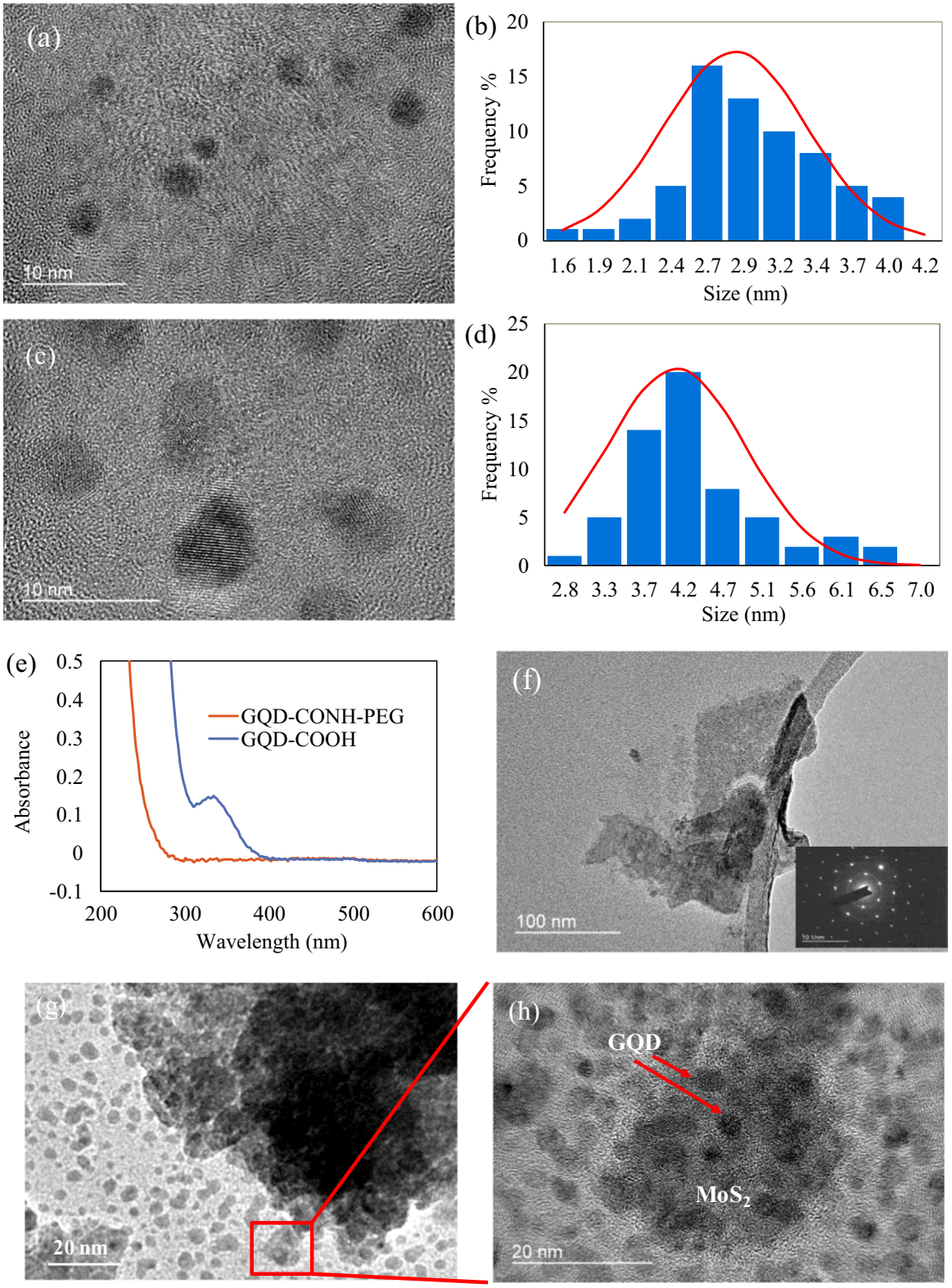

Fig. 1. (a) TEM image of bare GQDs; (b) Bare GQDs have an average size of 2.8 ± 0.5 nm; (c) TEM image of PEGlyted GQDs; (d) PEGlyted GQDs have an average size of 4.2 ± 0.8 nm; (e) UV–vis absorption spectra of GQDs before and after PEGylation; (f) TEM image of MoS_2 nanosheets. (Inset: SAED pattern taken on the MoS_2 flakes); (g) TEM image of the GQD-PEG-aptamer/MoS_2 nanosheet composite; (h) An enlarged HRTEM image of the selected area in (g).

adsorption of GQD labelled aptamer on MoS_2 nanosheets, which brought GQDs close enough to MoS_2 nanosheets to trigger the energy transfer from GQDs to MoS_2 nanosheets. The energy transfer efficiency is calculated by the equation of $QE=(F_0-F_q)/F_0$, where F_0 stands for the original fluorescence signal of control group (50 μL of GQD-PEG-aptamer solution with 50 μL of PBS), and F_q is the fluorescence intensity of GQD-PEG-aptamer after quenching by MoS_2 nanosheets. The calculated quenching efficiency and normalized fluorescence intensity is shown in Fig. 3b. The fluorescence quenching efficiency reached a maximum of

Please cite this article as: Shi, J., et al., Biosensors and Bioelectronics (2016), http://dx.doi.org/10.1016/j.bios.2016.09.012

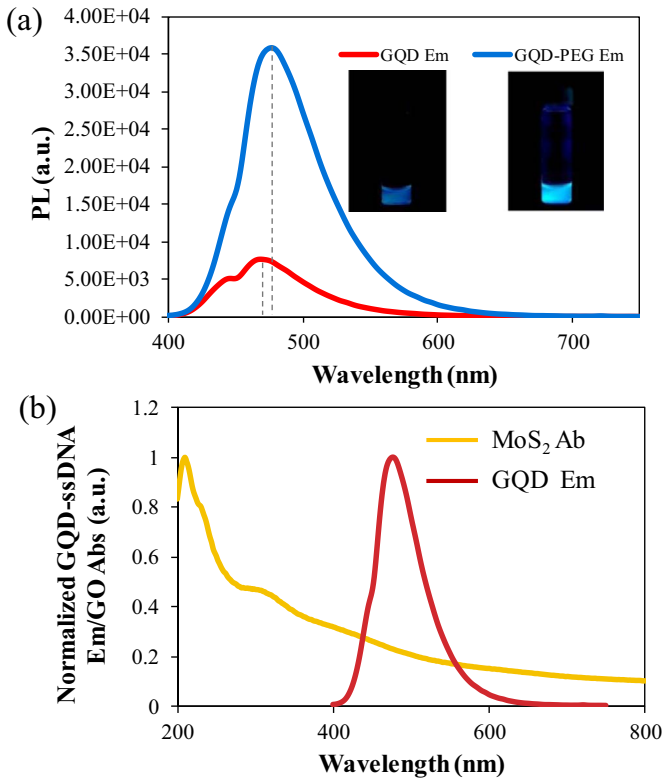

Fig. 2. (a) PL spectra of GQDs and GQDs-PEG dispersed in water. Inset: photographs of GQDs and GQDs-PEG in water; (b) Spectra overlapping between emission spectrum of GQDs and absorption spectra of MoS_2.

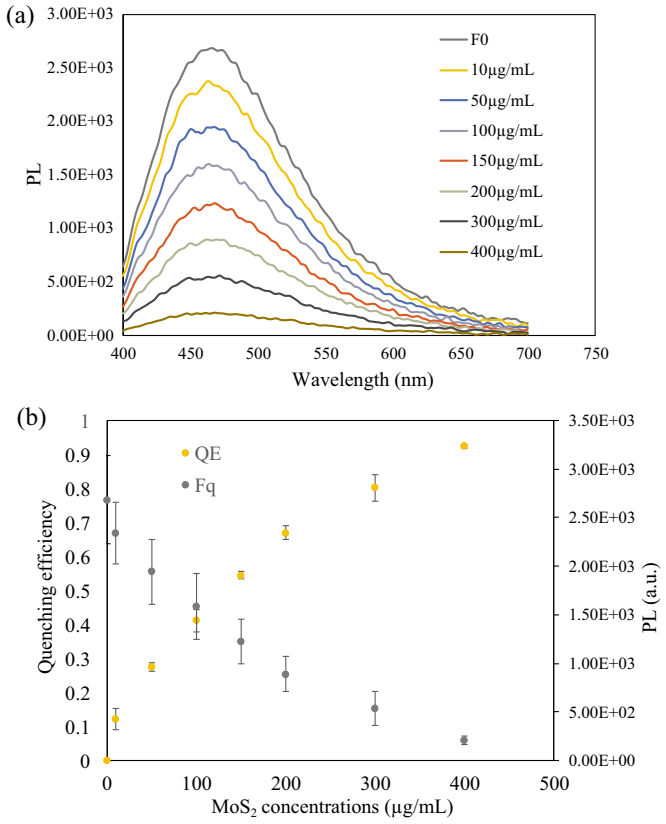

Fig. 3. (a) Fluorescence quenching spectra of GQD-PEG-aptamer with addition of increasing concentrations of MoS_2 nanosheets ranging from 10 to 400 μg/mL; (b) Quenching efficiency $QE=(F_0-F_q)/F_q$ and normalized PL intensity versus a series of MoS_2 nanosheet concentrations.

92.3% and the normalized fluorescence intensity (F_q/F_0) decreased to a minimum of 7.6% when the donor-to-acceptor ratio was 2.5. This high quenching efficiency verified the excellent quenching ability of MoS_2 nanosheets. Fig. S5 shows the MoS_2 quenching efficiency on bare GQD, GQD-PEG and GQD-PEG-aptamer. It was observed that there was a certain degree of quenching of bare GQD with MoS_2 nanosheets due to the physical adsorption between GQDs and MoS_2 nanosheets. When GQD was conjugated with PEG, an obvious lower quenching was observed due to the decrease of physical adsorption of GQD-PEG on MoS_2 surface. GQD-PEG-apatamer showed the highest quenching efficiency with MoS_2 nanosheet due to the strong hydrophobic adsorption of apatamer on MoS_2 nanosheet. The results demonstrated that the PEG passivation on GQD could largely decrease the unfavored physical adsorption of GQD on MoS_2 surface.

3.5. Detection of EpCAM

After investigating the quenching efficiency of MoS_2 nanosheets on GQD, GQD-PEG-aptamer/MoS_2 based sensing platform was utilized for the detection of EpCAM protein. In order to achieve optimal sensing performance, GQD-PEG-aptamer/MoS_2 based nanocomplex was prepared by using MoS_2 nanosheets with the concentration of 400 μg/mL, which ensured the maximum quenching efficiency (92.3%) and lowest background signal. As shown in Fig. S6, the response time of our nanobiosensor for EpCAM protein detection was around 50 min. Therefore, fluorescence emission spectra of GQD-PEG-aptamer/MoS_2 with incubation of EpCAM around 1 h were measured to quantify the fluorescence recovery signals. Fig. 4a shows averaged PL spectra of GQD-PEG-

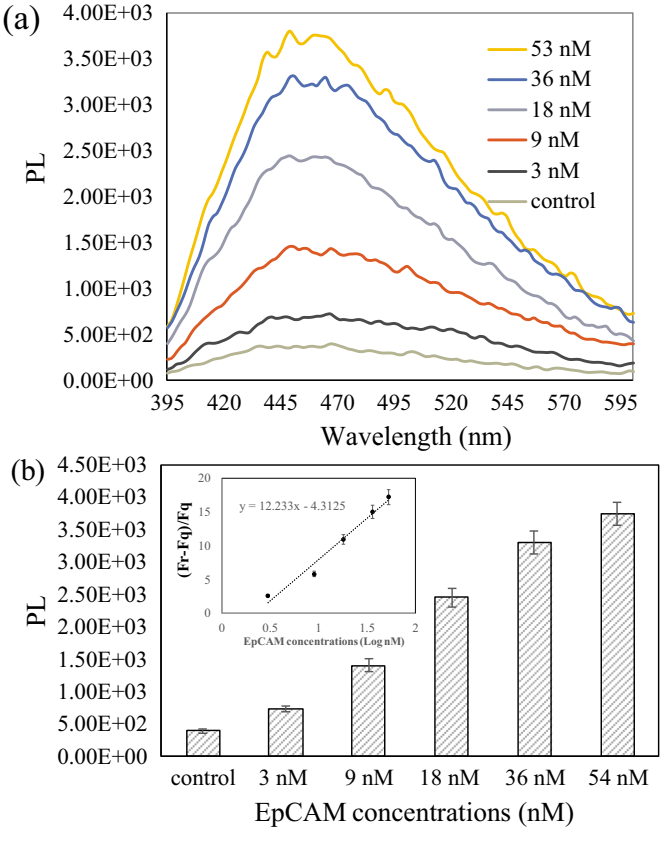

Fig. 4. (a) Fluorescence recovery spectra of GQD-PEG-aptamer/MoS_2 based sensing platform in addition of target EpCAM protein with various concentrations from 3 nM to 54 nM; (b) The recovered peak fluorescence signal versus a series of concentrations of target EpCAM protein. Inset is the fitting logarithmic curve between relative peak fluorescence signal and the EpCAM concentrations.

aptamer/MoS_2 composite against increasing concentrations of target EpCAM protein. It was observed that the emission spectra of GQD gradually recovered with the increasing concentrations of target EpCAM protein. The maximum fluorescence signal change between two adjacent spectra curves was at the spectra peak around 478 nm. Therefore, the following fluorescence recovery signal analysis was based on spectra peak signals. The fluorescence recovery reason was that the stronger affinity interaction between aptamer and target EpCAM protein detached GQD labelled aptamer from MoS_2 nanosheet surface. As the distance between GQDs as donors and the MoS_2 nanosheets as acceptors increased, the fluorescence signals were recovered due to the disappearance of FRET effect.

Fig. 4b shows the fluorescence peak signal of the nanosensor with the change of EpCAM concentrations. To further analyze the fluorescence recovery of this nanobiosensor, the relative recovery rate $((F_r-F_q)/F_q)$ is used. Where F_r is the recovered fluorescence intensity after addition of target EpCAM protein, and F_q is the fluorescence intensity of prepared GQD-aptamer-PEG/MoS_2 assay after quenching. As shown in the inlet of Fig. 4b, a linear curve was obtained between relative fluorescence signal recovery rate and logarithmic concentrations with the equation of $y=12.233x-4.3125$, where y is the relative fluorescence peak signal recovery rate. The limit of detection (LOD) for EpCAM detection is calculated as 450 pM based on the control group signal plus 3 times of standard derivation. The current available methods for EpCAM protein detection include immunoassays (Schmetzer et al., 2012; Seeber et al., 2015), electrochemical sensor (Ortega et al., 2015) and fluorescence sensor (Jung et al., 2014) with LOD from single-digit pM to hundreds of pM. As a proof of concept, our nanobiosensor achieved a LOD around 450 pM which was comparable to the immunoassays and sensors reported in the literature. Moreover, the current approaches are mainly based on anti-EpCAM antibody, which is expensive and not stable in the sensing environment. Our aptamer based nanobiosensor has the potential to be a cheap and stable platform for cancer biomarker detection.

To evaluate the specificity of this biosensor for EpCAM protein detection, the responses of this biosensor with bovine serum albumin (BSA) and immunoglobulin G (IgG) and EpCAM with the same concentration of 54 nM were tested. The other experimental conditions were the same with the previous description. For comparison, all the measured PL signals were normalized based on that in PBS solution. As shown in Fig. 5a, no obvious fluorescence recovery signals were observed for BSA and IgG. The experimental results indicated that this detection system had a good specificity for EpCAM detection.

To demonstrate the feasibility of this biosensor for real cancer cell sample detection, breast cancer cell line MCF-7 expressed with EpCAM was used as the target. GQD-PEG-aptamer/MoS_2 composite (200 μg/mL) was incubated with MCF-7 cells with a concentration of 1.0×10^5 cells/mL for 2 h. As shown in Fig. 5b, there was no obvious fluorescence signal when GQD-PEG-aptamer/MoS_2 composites were just added to MCF cells due to the FRET effect between GQD-aptamer and MoS_2. After 2-h incubation, blue fluorescence labelled MCF-7 cells were clearly observed due to the stronger binding between MCF-7 cells and GQD labelled aptamers, leading to the detachment of GQD labelled aptamers from MoS_2 nanosheets and conjugation with MCF-7 cells. These results demonstrated the potential of this nanobiosensor for EpCAM expressed cancer cell detection.

4. Conclusion

In this paper, a novel FRET biosensor based on GQD-PEG-aptamer and MoS_2 nanosheet pairs was developed for EpCAM

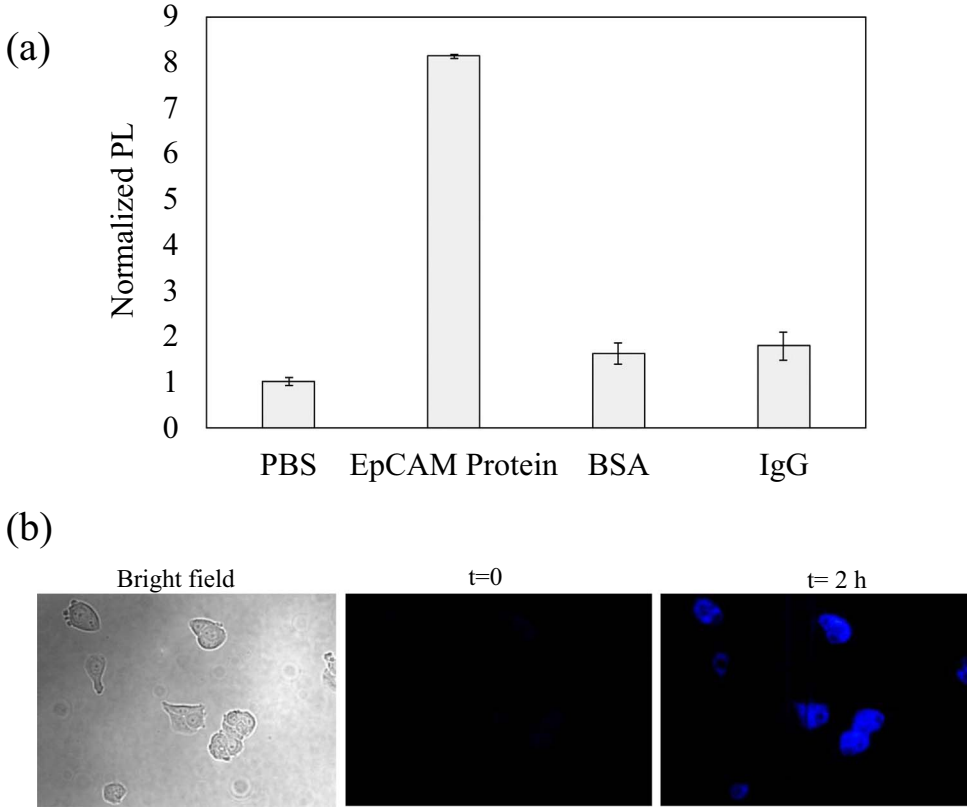

Fig. 5. (a) Specificity testing of this nanobiosensor with BSA and IgG proteins as control groups. (b) MCF-7 cell detection experiments (bright field image of cultured MCF-7 cells and fluorescence image of MCF-7 cells before and after incubation with GQD-aptamer-MoS_2 composite for 2 h.).

Please cite this article as: Shi, J., et al., Biosensors and Bioelectronics (2016), http://dx.doi.org/10.1016/j.bios.2016.09.012

protein detection. The FRET assay was established by the adsorption of GQD-PEG-aptamer on MoS_2 nanosheets via van der walls force, which brought GQDs and MoS_2 into close proximity to trigger FRET phenomena. PEGylated GQDs showed much higher fluorescence emission intensity compared with bare GQDs. The established FRET assay was successfully used for EpCAM protein detection with a logarithmic linear detection range from 3 nM to 54 nM and a limit of detection of 450 pM. This nanobiosensor was also successfully used for EpCAM expressed breast cancer MCF-7 cell detection, which could be a promising tool for cancer biomarker and EpCAM expressed cancer cell detection.

Acknowledgements

This work was supported by the Hong Kong Research Council General Research Grant (PolyU 152213/15E), the Hong Kong Ph.D Fellowship Scheme Fund (HKPF14-14076/PolyU RUD4) and the internal fund of the Hong Kong Polytechnic University (G-YBAA).

Appendix A. Supporting information

Supplementary data associated with this article can be found in the online version at http://dx.doi.org/10.1016/j.bios.2016.09.012.

References

Armstrong, A., Eck, S.L., 2003. Cancer Biol. Ther. 2, 320–325.
Ataca, C., Ciraci, S., 2011. J. Phys. Chem. C 115, 13303–13311.
Baeuerle, P.A., Gires, O., 2007. Br. J. Cancer 96, 417–423.
Bagalkot, V., Zhang, L., Levy-Nissenbaum, E., Jon, S., Kantoff, P.W., Langery, R., Farokhzad, O.C., 2007. Nano Lett. 7, 3065–3070.
Bhatnagar, D., Kumar, V., Kumar, A., Kaur, I., 2016. Biosens. Bioelectron. 79, 495–499.
Choi, J.H., Chen, K.H., Strano, M.S., 2006. J. Am. Chem. Soc. 128, 15584–15585.
Dalerba, P., Dylla, S.J., Park, I.-K., Liu, R., Wang, X., Cho, R.W., Hoey, T., Gurney, A., Huang, E.H., Simeone, D.M., Shelton, A. a, Parmiani, G., Castelli, C., Clarke, M.F., 2007. Proc. Natl. Acad. Sci. USA 104, 10158–10163.
Deng, H.M., Yang, X.J., Gao, Z.Q., 2015. Analyst 140, 3210–3215.
Fong, D., Steurer, M., Obrist, P., Barbieri, V., Margreiter, R., Amberger, a, Laimer, K., Gastl, G., Tzankov, a, Spizzo, G., 2008. J. Clin. Pathol. 61, 31–35.
Gastl, G., Spizzo, G., Obrist, P., Dünser, M., Mikuz, G., 2000. Lancet 356, 1981–1982.
Ge, J., Ou, E.C., Yu, R.Q., Chu, X., 2014. J. Mater. Chem. B 2, 625–628.
Gubala, V., Harris, L.F., Ricco, A.J., Tan, M.X., Williams, D.E., 2012. Anal. Chem. 84, 487–515.
Jung, Y.K., Woo, M.A., Soh, H.T., Park, H.G., 2014. Chem. Commun. 50, 12329–12332.
Kong, R.M., Ding, L., Wang, Z., You, J., Qu, F., 2015. Anal. Bioanal. Chem 407, 369–377.
Lambrechts, A.C., Bosma, A.J., Klaver, S.G., Top, B., Perebolte, L., van't Veer, L.J., Rodenhuis, S., 1999. Breast Cancer Res. Treat. 56, 219–231.
Ntouroupi, T.G., Ashraf, S.Q., McGregor, S.B., Turney, B.W., Seppo, A., Kim, Y., Wang, X., Kilpatrick, M.W., Tsipouras, P., Tafas, T., Bodmer, W.F., 2008. Br. J. Cancer 99, 789–795.
Ortega, F.G., Fernandez-Baldo, M.A., Serrano, M.J., Messina, G.A., Lorente, J.A., Raba, J., 2015. Sens. Actuators B: Chem. 221, 248–256.
Qian, Z.S., Shan, X.Y., Chai, L.J., Chen, J.R., Peng, H., 2015. Biosens. Bioelectron. 68, 225–231.
Schmetzer, O., Moldenhauer, G., Nicolaou, A., Schlag, P., Riesenberg, R., Pezzutto, A., 2012. Immunol. Lett. 143, 184–192.
Schwartzberg, L.S., 2001. Crit. Rev. Oncol. Hematol. 40, 17–24.
Seeber, A., Martowicz, A., Spizzo, G., Buratti, T., Obrist, P., Fong, D., Gastl, G., Untergasser, G., 2015. BMC Cancer 15, 372.
Shen, J.H., Zhu, Y.H., Chen, C., Yang, X.L., Li, C.Z., 2011. Chem. Commun. 47, 2580–2582.
Shi, J.Y., Tian, F., Lyu, J., Yang, M., 2015a. J. Mater. Chem. B 3, 6989–7005.
Shi, J.Y., Chan, C., Pang, Y., Ye, W., Tian, F., Lyu, J., Zhang, Y., Yang, M., 2015b. Biosens. Bioelectron. 67, 595–600.
Shi, J.Y., Guo, J., Bai, G., Chan, C., Liu, X., Ye, W., Hao, J., Chen, S., Yang, M., 2015c. Biosens. Bioelectron. 65, 238–244.
Song, Y., Zhu, Z., An, Y., Zhang, W., Zhang, H., Liu, D., Yu, C., Duan, W., Yang, C.J., 2013. Anal. Chem. 85, 4141–4149.
Sun, H., Wu, L., Wei, W., Qu, X., 2013. Mater. Today 16, 433–442.
Tan, W., Donovan, M.J., Jiang, J., 2013. Chem. Rev. 113, 2842–2862.
Tsang, M.K., Ye, W.W., Wang, G.J., Li, J.M., Yang, M., Hao, J.H., 2016. ACS Nano 1, 598–605.
Varga, M., Obrist, P., Schneeberger, S., Mu, G., Felgel-farnholz, C., Fong, D., Zitt, M., Brunhuber, T., 2004. Clin. Cancer Res. 10, 3131–3136.
Xu, M., Liang, T., Shi, M., Chen, H., 2013. Chem. Rev. 113, 3766–3798.
Yamashita, T., Ji, J., Budhu, A., Forgues, M., Yang, W., Wang, Y., Jia, H., Ye, Q., Qin, L., Wauthier, E., Reid, L.M., Minato, H., Honda, M., Kaneko, S., Tang, Z., Wang, X.W., 2010. NIH Public Access 136, 1012–1024.
Yang, G.H., Zhu, C.Z., Du, D., Zhu, J.J., Lin, Y.H., 2015. Nanoscale 7, 14217.
Ye, W.W., Tsang, M.K., Liu, X., Yang, M., Hao, J., 2014. Small 10, 2390–2397.
Zhang, C.-Y., Yeh, H.-C., Kuroki, M.T., Wang, T.-H., 2005. Nat. Mater. 4, 826–831.
Zhu, C., Zeng, Z., Li, H., Li, F., Fan, C., Zhang, H., 2013. J. Am. Chem. Soc. 135, 5998–6001.
Zhu, S., Zhang, J., Tang, S., Qiao, C., Wang, L., Wang, H., Liu, X., Li, B., Li, Y., Yu, W., Wang, X., Sun, H., Yang, B., 2012. Adv. Funct. Mater. 22, 4732–4740.

Please cite this article as: Shi, J., et al., Biosensors and Bioelectronics (2016), http://dx.doi.org/10.1016/j.bios.2016.09.012